Biochars prepared from rabbit manure for the adsorption of rhodamine B and Congo red: characterisation, kinetics, isotherms and thermodynamic studies

Wen Huang, Min Zhang, Yinhai Wang, Jiao Chen and Jianqiang Zhang

ABSTRACT

Biochar was prepared from rabbit faeces (RFB_{550}) at 550 °C through pyrolysis and was characterised using elemental analysis, scanning electron microscopy, Brunauer–Emmett–Teller analysis and Fourier transform infrared spectroscopy (FTIR). The related factors, kinetics, isothermal curves and thermodynamics of the adsorption behaviours were investigated by conducting batch experiments. The results revealed the adsorption equilibrium of rhodamine B (RhB) and Congo red (CR) onto RFB_{550} with initial concentrations of 30 $mg \cdot L^{-1}$ at 25 °C and 210 min, and the best adsorption was observed when the pH of the RhB and CR solutions was 3 and 5, respectively. Pseudo-second-order kinetics was the most suitable model for describing the adsorption of RhB and CR onto RFB_{550}, indicating that the rate-limiting step was mainly chemical adsorption. The isotherm data were best described by the Freundlich model, and the adsorption process was multi-molecular layer adsorption. Thermodynamic parameters revealed the spontaneous adsorption of RhB and CR onto RFB_{550}. According to the results of the FTIR analysis, the oxygen-containing functional groups and aromatic structures on the surface of RFB_{550} provided abundant adsorption sites for RhB and CR, and the adsorption mechanism was potentially related to the hydrogen bonds and π–π bonds.

Key words | biochar, isotherms, kinetics, rabbit faeces, thermodynamics

Wen Huang
Min Zhang
Yinhai Wang
Jianqiang Zhang (corresponding author)
Faculty of Geosciences and Environmental Engineering,
Southwest Jiaotong University,
Chengdu 611756,
China
E-mail: *zhjiqicn@swjtu.cn*

Jiao Chen
Department of Architectural and Environmental Engineering,
Chengdu Technological University,
Chengdu 610031,
China

INTRODUCTION

Dyes are widely used in the textile, paper, medicine, food and plastic industries due to their low cost, stable nature and variety. Dyes are poorly biodegradable, highly toxic and have a complex composition and deep colours. At the same time, most dyes and their metabolic intermediates possess mutagenic and carcinogenic potential, as well as other characteristics (Khattri & Singh 2009). Wastewater that contains dyes does not easily meet the emission requirements after biological treatment. Thus, the extensive use of dyes causes a human health concern and water pollution. To date, several methods have been developed to remove dyes from aqueous solutions, such as adsorption (Cheng *et al.* 2018; Zhang *et al.* 2018), advanced oxidation (Dawood & Sen 2012) and membrane separation (Baslak *et al.* 2016). Activated carbon adsorption has exhibited good performance in removing dyes; however, its application has been restricted by its high cost. The identification of new adsorption materials that are cleaner, more efficient and inexpensive has therefore become a research hotspot in recent years.

Biochar is a carbonaceous material produced by pyrolysis of biomass under limited or absence of oxygen conditions. Its highly aromatic structure and abundance of oxygen-containing functional groups endow the biochar with good adsorption sites and stability. Recently, several studies examining the adsorption of dyes by biochar have been reported. However, these studies primarily used Korean cabbage (Sewu *et al.* 2017), straw (Lian *et al.* 2016), *Pongamia glabra* seed cover (Bordoloi *et al.* 2018) and other plants as raw materials to prepare biochar, but its preparation from animal manure as the source material for dye adsorption has rarely been reported. The adsorption properties and mechanism by which biochar adsorbs different types of dyes have not been clearly elucidated. This study therefore used rabbit faeces as the raw material to prepare a biochar for the adsorption rhodamine B (RhB) and Congo red (CR). The effects of the solution pH, biochar concentration, adsorption time and temperature on the adsorption effect were investigated. Based on this information, the adsorption

doi: 10.2166/wst.2020.100

mechanism was analysed using kinetic, isothermal and thermodynamic models to provide a theoretical basis for the targeted selection of animal-derived biochar applications.

MATERIALS AND METHODS

Materials

Biomass waste solids of rabbit faeces were collected from a rabbit farm in Pixian, Chengdu. RhB and CR were purchased from Tianjin Ruijin Special Chemical Co. Stock solutions of 1,000 mg · L^{-1} RhB and CR were prepared and diluted to the required concentration (5–250 mg · L^{-1}). The initial pH of the RhB and CR solutions was adjusted by adding 1 · L^{-1} sodium hydroxide (NaOH) and 1 mol/L hydrochloric acid (HCl) solutions. All the reagents used in the experiment were analytically pure, and the water used in this study was deionised water.

Preparation of biochar

The rabbit faeces were ground through an 80-mesh sieve after drying and removing the impurities. Appropriate amounts of sifted materials were weighed, placed into a crucible, compacted and covered, and then placed in a stainless steel cylinder. The air in the cylinder was removed by purging it with nitrogen gas to ensure an oxygen-free atmosphere, and the cylinder was then placed in the furnace. The temperature was further increased to 550 °C at a rate of approximately 15 °C per minute and incubated for 150 min. After cooling to room temperature, 20 mL of HCl (1.0 mol/L) was added to the resulting material in 1:25 solid:liquid ratio (m:V), and the solution was shaken at 150 rpm for 30 min. The products were rinsed with deionised water to achieve a neutral pH and the process was repeated three times to remove the ash. Finally, the products were dried at 100 °C for 48 h and then passed through a 100-mesh sieve. Based on the charring temperature, the rabbit faeces biochar was labelled as RFB_{550}.

Biochar characterisation

The contents of carbon (C), hydrogen (H), nitrogen (N) and oxygen (O) were measured using an elemental analyser. The surface physical morphology of RFB_{550} was observed using a scanning electron microscope (SEM). The surface area and porosity of RFB_{550} were determined using the Brunauer–Emmett–Teller (BET) method. The functional groups on the surface of RFB_{550} were determined using Fourier transform infrared spectroscopy (FTIR).

Adsorption experiments

Adsorption experiments were conducted using a 250 mL Erlenmeyer flask and 100 mL of 30 mg · L^{-1} RhB and CR solutions.

1. pH effect: For this experiment, 1 mol · L^{-1} HCl or NaOH was added to the RhB and CR solutions to adjust the pH to 3–11. Then, 0.07 g of RFB_{550} was added to each solution with different pH values. The pH of the RhB and CR solutions was adjusted to 3 and 5, respectively, in subsequent experiments.
2. Effect of the biochar concentration: Different concentrations of RFB_{550} were added to prepare solutions with liquid:solid ratios ranging from 0.7 to 2 g · L^{-1}.
3. Effect of the contact time: First, 0.09 g or 0.15 g RFB_{550} was added to RhB and CR solutions with a concentration of 30 mg · L^{-1}. Next, samples were analysed at 10, 30, 50, 70, 90, 120, 150, 210, 300, 400 and 500 min.
4. Temperature effect: For this experiment, 0.09 g or 0.15 g RFB_{550} was added to RhB and CR solutions. The samples were placed in an oscillating shaker operated at 180 rpm for 210 min. The experiment was conducted at 5 °C, 15 °C, 25 °C, 35 °C and 45 °C. After shaking, the suspensions were centrifuged at 4,000 rpm for 5 min and the absorbance of the clear solution was measured using a spectrophotometer (the wavelengths were set to 554 nm and 499 nm respectively, UV-1800PC, HITACHI, Japan).

Adsorption kinetics

Based on the parameters observed from the experiments described above, the pH of the RhB and CR solutions was adjusted to 3 and 5, respectively, and 0.09 g and 0.15 g RFB_{550} were added to different initial concentrations (30 and 60 mg · L^{-1}) of RhB and CR. All samples were analysed at 10, 30, 50, 70, 90, 120, 150, 210, 300, 400 and 500 min. The other steps were the same as described above. The amounts of adsorbed RhB and CR (q_t, mg · g^{-1}) and removal rates (η, %) were calculated using Equations (1) and (2), respectively. The adsorption kinetic models are shown in Equations (3)–(6) (Yang & Jiang 2014).

$$q_t = (C_0 - C_t)V/m \quad (1)$$

$$\eta = (C_0 - C_t) \times 100\%/C_0 \quad (2)$$

where C_0 and C_t are the initial and equilibrium concentrations of RhB and CR, respectively, in mg · L^{-1}; V is the

volume of the solution in mL; and m is the mass of the biochar in g.

Pseudo-first-order kinetic model:

$$\ln(q_e - q_t) = \ln q_e - k_1 t \tag{3}$$

Pseudo-second-order kinetic model:

$$\frac{t}{q_t} = \frac{t}{q_e} + \frac{1}{k_2 q_e^2} \tag{4}$$

Intra-particle diffusion model:

$$q_t = k_3 t^{0.5} + \mathrm{C} \tag{5}$$

Elovich model:

$$q_t = A + B \ln t \tag{6}$$

where q_e ($\mathrm{mg \cdot g^{-1}}$) is equilibrium amount of RhB and CR adsorbed; q_t ($\mathrm{mg \cdot g^{-1}}$) is the amount of RhB and CR adsorbed at time t; k_1 ($\mathrm{min^{-1}}$), k_2($\mathrm{g \cdot (mg \cdot min)^{-1}}$) and k_3 ($\mathrm{mg \cdot (g \cdot min^{0.5})^{-1}}$) are the rate constants of the pseudo-first-order, pseudo-second-order and intra-particle diffusion models, respectively; t (min) is the contact time; and A, B and C are correlation constants.

Adsorption isotherm and thermodynamic models

In the present study, the pH of the RhB and CR solutions was adjusted to 3 and 5, respectively, and 0.09 g and 0.15 g RFB_{550} were added to different initial concentrations of RhB and CR (20, 30, 40, 50, 60 and 80 $\mathrm{mg \cdot L^{-1}}$). The flasks were agitated at 180 rpm for 210 min at 25 °C, 35 °C and 45 °C. The other steps were the same as described above. The adsorption isotherm model is shown in Equations (7) and (8), and the adsorption thermodynamic model is shown in Equations (9) and (10) (Mandal *et al.* 2017).

$$\text{Langmuir model: } q_e = \frac{q_m K_L C_e}{1 + K_L C_e} \tag{7}$$

$$\text{Freundlich model: } q_e = K_F C_e^{1/n} \tag{8}$$

where q_e ($\mathrm{mg \cdot g^{-1}}$) is the equilibrium amounts of RhB and CR adsorbed; q_m ($\mathrm{mg \cdot g^{-1}}$) is the theoretical maximum amount of RhB and CR adsorbed, respectively; C_e ($\mathrm{mg \cdot L^{-1}}$) is the RhB and CR concentration at equilibrium; K_L ($\mathrm{L \cdot mg^{-1}}$) and K_F ($\mathrm{mg \cdot g^{-1}(mg \cdot L^{-1})^{-n}}$) are equilibrium constants for the Langmuir and Freundlich model, respectively; and $1/n$ is the index of the Freundlich model.

$$\Delta G^{\theta} = -RT \ln K_e \tag{9}$$

$$\Delta G^{\theta} = \Delta H^{\theta} - T\Delta S^{\theta} \tag{10}$$

where R ($8.314\ \mathrm{J \cdot (mol \cdot K)^{-1}}$) is the ideal gas constant; T is the temperature in Kelvin(K); ΔG^{θ}($\mathrm{kJ \cdot mol^{-1}}$) is the change in the Gibbs free energy; ΔH^{θ}($\mathrm{kJ \cdot mol^{-1}}$) is the change in enthalpy; ΔS^{θ}($\mathrm{kJ \cdot (mol \cdot K)^{-1}}$) is the change in entropy; and K_e is the thermodynamic constant.

RESULTS AND DISCUSSION

Biochar characterisation

The elemental composition of RFB_{550} is presented in Table 1. RFB_{550} contains a large amount of C and lower levels of H, O and N. Generally, the aromaticity and carbonisation level of the adsorbate are determined according to the H/C ratio, and adsorbate polarity is generally determined by the O/C and (O + N)/C ratios. (Schimmelpfennig & Glaser 2012). A lower H/C ratio indicates a higher carbonation level and aromaticity, and higher O/C and (O + N)/C ratios indicate an increase in the polarity of the biochar. In this study, H/C < 0.6 and O/C < 2.0, indicating that RFB_{550} had high aromaticity and stability. The BET surface area, total pore volume and average pore diameter of RFB_{550} were $42.66\ \mathrm{m^2 \cdot g^{-1}}$, $0.138\ \mathrm{cm^3 \cdot g^{-1}}$ and 9.91 nm, respectively. The SEM images of RFB_{550} are shown in Figure 1. The surface of RFB_{550} was rough and

Table 1 | Elemental composition and BET analysis of RFB_{550}

Property		Value
Mass composition	Ash content/%	17.18
	C/%	63.22
	H/%	2.98
	O/%	6.52
	N/%	2.22
Atomic ratio	H/C	0.047
	O/C	0.10
	(O + N)/C	0.145
Surface area ($\mathrm{m^2 \cdot g^{-1}}$)		42.66
Total pore volume ($\mathrm{cm^3 \cdot g^{-1}}$)		0.138
Average pore diameter (nm)		9.91

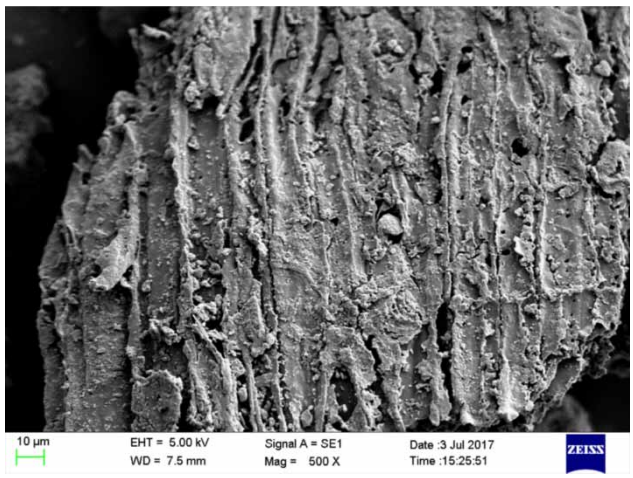

Figure 1 | SEM morphology of RFB_{550}.

uneven, with a large number of irregular pores per unit area. As a result, the stronger aromaticity and polarity, large specific surface area and rich pore structure of RFB_{550} provides favourable conditions for RhB and CR adsorption onto RFB_{550}.

Preliminary adsorption studies

Effect of pH on adsorption

The pH of the solution is an important factor affecting the adsorption process because it not only alters the surface protonation state of the adsorbent but also affects the speciation of the adsorbate. The effects of different initial solution pH values on the adsorption of RhB and CR onto RFB_{550} are shown in Figure 2(a). The removal rate of RhB by RFB_{550} decreased as the pH increased. Under acidic conditions, the surface functional groups of RFB_{550} were highly protonated and the adsorption effect was increased by ion exchange with RhB quaternary ammonium cations or molecules in solution. Under alkaline conditions, RFB_{550} was deprotonated and the RhB in the solution underwent carboxyl ionisation, resulting in the production of an amphoteric compound containing both a quaternary ammonium cation and carboxyl anion. The mutual polymerisation or precipitation between RhB leads to poor adsorption (Li *et al.* 2010; Almasi *et al.* 2012). At pH5, the sulfonic acid group of CR ($-SO_3Na$) will be hydrolysed into a

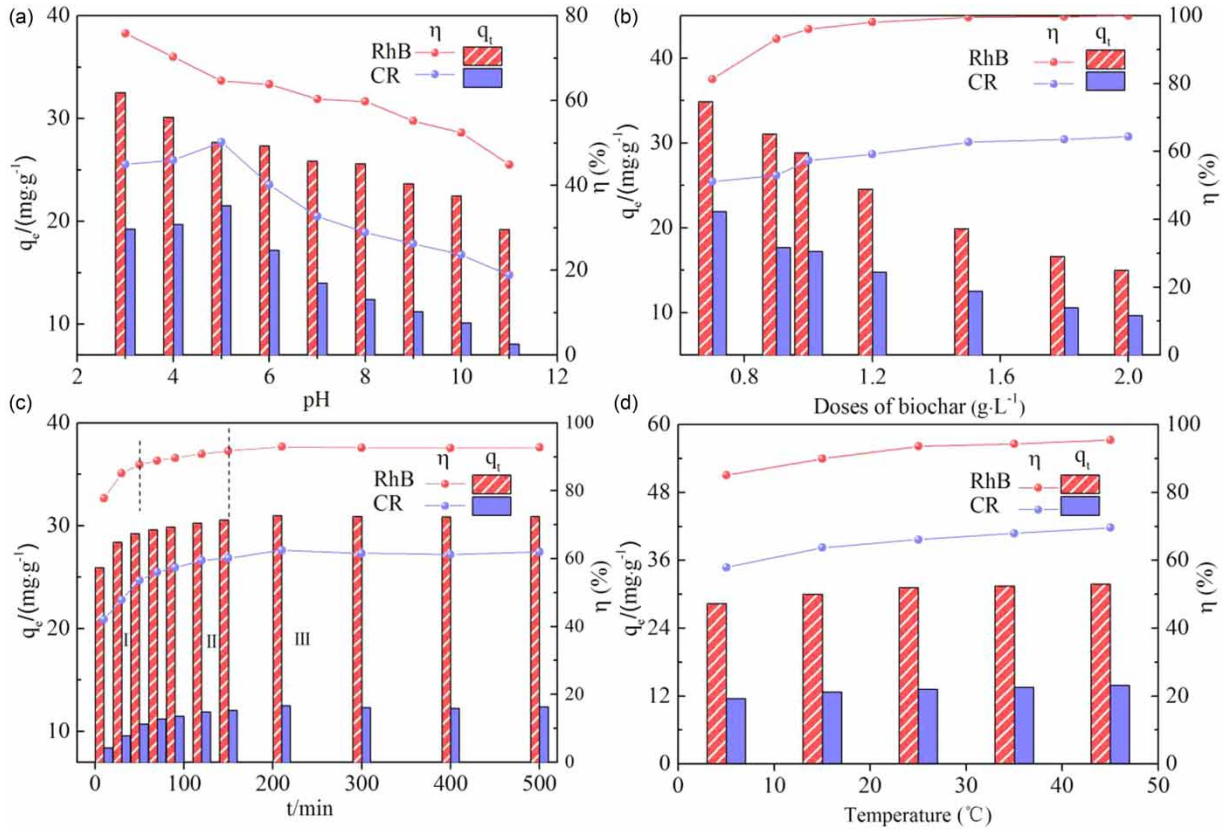

Figure 2 | Effects of different variables on adsorption efficiency (a) solution pH, (b) biochar concentration, (c) contact time, and (d) temperature.

negatively charged ion ($-SO_3^-$) and the surface functional groups of RFB_{550} become protonated (Ahmad & Kumar 2010; Zhang *et al.* 2011), Therefore, the best adsorption effect was mediated by electrostatic attraction. However, as the pH increased the protonation of RFB_{550} and electrostatic attraction gradually decreased, resulting in a decrease in the removal rate. Therefore, the optimal pH values for RhB and CR adsorption by RFB_{550} are 3 and 5, respectively.

Effect of the biochar concentration

The effects of different RFB_{550} concentrations on RhB and CR adsorption are shown in Figure 2(b). According to the results, the RhB and CR removal rates of RFB_{550} increased and then tended to plateau as the RFB_{550} concentration increased, which was related to the increases in the specific surface area and active adsorption sites for RhB and CR as the biochar concentration increased. In contrast, the RhB and CR adsorption capacity of RFB_{550} decreased as the RFB_{550} concentration increased. When the concentration of RFB_{550} increased from 0.7 to $2\,g\cdot L^{-1}$, the adsorption capacity for RhB and CR decreased from 34.87 to $15.00\,mg\cdot g^{-1}$ and 21.92 to $9.65\,mg\cdot g^{-1}$, respectively. An excess concentration of RFB_{550} decreased the equilibrium concentrations of RhB and CR in the liquid phase, and the amounts of RhB and CR adsorbed decreased per unit mass of RFB_{550}.

Effect of contact time

The effects of contact time on RhB and CR removal are shown in Figure 2(c). The adsorption process was divided into three stages: I, rapid adsorption phase (10–50 min); II, slow diffusion phase (50–180 min) and III, adsorption equilibrium phase (180–500 min). In the rapid adsorption phase, the adsorption sites of RFB_{550} were abundant and the highest concentrations of RhB and CR were adsorbed. RhB and CR quickly occupied the active sites through the action of mass transfer, and thus the highest removal rates were achieved. At this stage, the amounts of RhB and CR adsorbed onto RFB_{550} reached 29.22 and $10.72\,mg\cdot g^{-1}$, respectively. In the slow diffusion phase, with an increase in the contact time, the surface active sites of RFB_{550} and the residual RhB and CR concentrations in the solution decreased; thus, the removal rate increased slowly with the reduction in the mass transfer driving force. In the adsorption equilibrium phase, the adsorption tends to be saturated, and the amount adsorbed and removal rate change little over time. At 180 min, the adsorption reached equilibrium and the amounts of RhB and CR adsorbed onto RFB_{550} were 30.99 and $12.50\,mg\cdot g^{-1}$, respectively.

Effect of temperature

The dye-containing wastewater, which is directly discharged from the actual printing and dyeing process, reaches temperatures greater than 80 °C. After heat recovery, the residual temperature is approximately 40 °C. An analysis of the characteristics of the adsorption of organic dyes onto biochar at higher temperatures is therefore crucial. Figure 2(d) shows the adsorption performance for RhB and CR onto RFB_{550} at different temperatures. When temperature increased from 5 to 45 °C, the amounts of RhB and CR adsorbed onto RFB_{550} increased from 28.36 to $31.84\,mg\cdot g^{-1}$ and 11.59 to $13.93\,mg\cdot g^{-1}$, respectively. Meanwhile, the corresponding removal rates increased from 85.09% to 95.53% and 57.93% to 69.63%, respectively. Based on these results, when the temperature increased, the porosity and total pore volume of the RFB_{550} and diffusion rate of RhB and CR increased, resulting in increases in the amounts of RhB and CR adsorbed and removal rates (Hameed & Ahmad 2009).

Adsorption kinetics

The kinetics of the adsorption of different initial concentrations of RhB and CR solutions (30 and $60\,mg\cdot L^{-1}$, respectively) were analysed using a pseudo-first-order, pseudo-second-order, intra-particle diffusion and Elovich models to further study the mechanism by which RFB_{550} adsorbs RhB and CR. The kinetic curves of RhB and CR adsorption onto RFB_{550} are presented in Figure 3 and the parameters are shown in Table 2. RhB and CR adsorption fitted best to the pseudo-second-order model with coefficient of correlation (R^2) greater than 0.90. The values of q_e calculated by fitting the equation were very close to the experimental q_e values, and the relative error was less than 4.67%. The pseudo-second-order kinetic model reflected the entire adsorption process, namely liquid film diffusion, surface adsorption and intra-particle diffusion (Fan *et al.* 2016). RhB and CR therefore probably adsorbed onto RFB_{550} through multiple mechanisms. The rate-limiting step was mainly chemical adsorption (Sun *et al.* 2014). The rate constant k_2 decreased with increasing initial concentrations of RhB and CR, indicating that mass transfer was more likely to occur at higher RhB and CR concentrations. Considering the results of the intra-particle diffusion model, the coefficient of correlation (R^2) increased as the

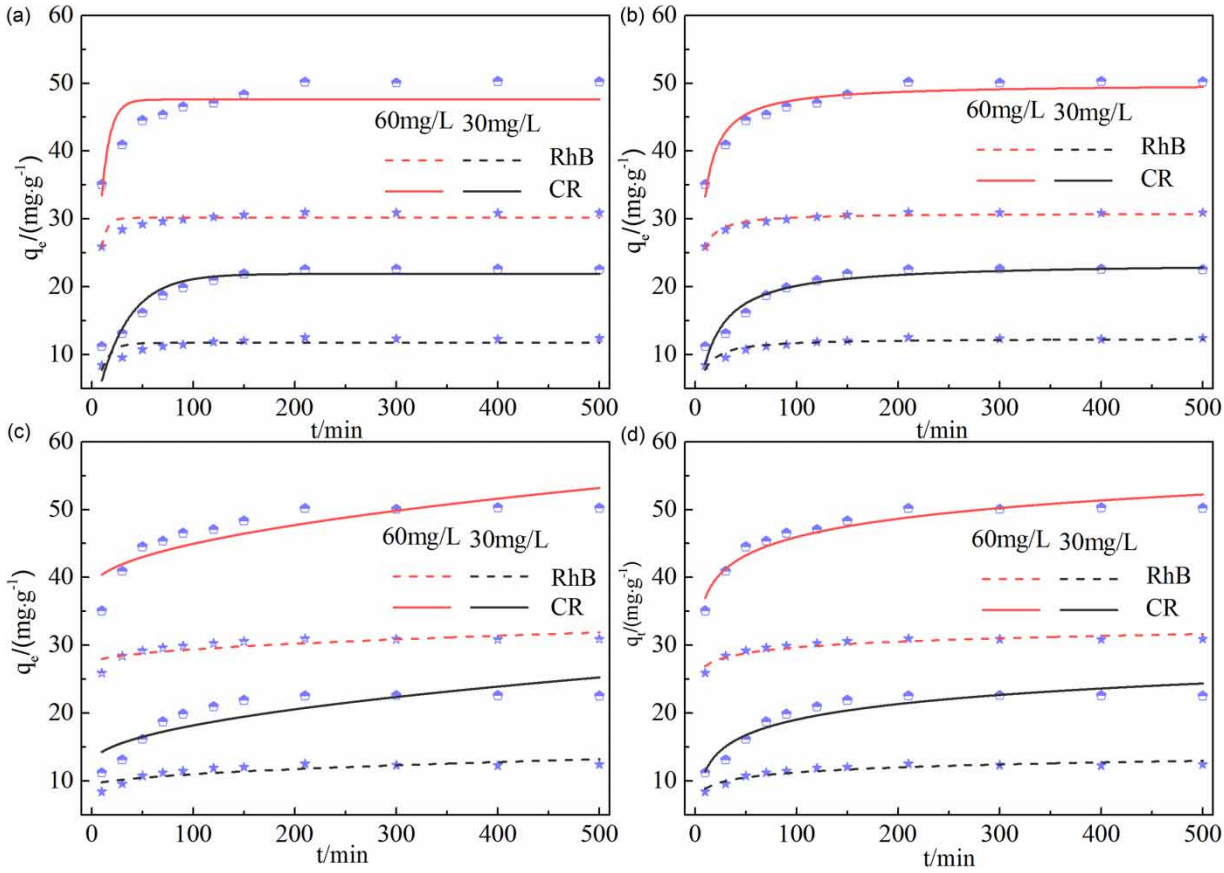

Figure 3 | Adsorption kinetics curves of RhB and onto RFB_{550} (a) pseudo-first-order model, (b) pseudo-second-order model, (c) intra-particle diffusion model, and (d) Elovich model.

Table 2 | Kinetic parameters for the adsorption of RhB and CR onto RFB_{550}

Initial concentration (·L^{-1})		Pseudo-first-order kinetic model			Pseudo-second-order kinetic model			Intra-particle diffusion model			Elovich model		
		q_e	k_1	R^2	q_e	k_2	R^2	C	k_3	R^2	A	B	R^2
20	RhB	30.182	0.193	0.6888	30.850	0.016	0.9504	27.371	0.202	0.6171	24.072	1.220	0.8740
	CR	11.738	0.108	0.5911	12.392	0.014	0.9058	9.2086	0.179	0.6609	6.3856	1.060	0.8921
60	RhB	47.608	0.122	0.6313	49.932	0.004	0.9272	38.308	0.666	0.7066	28.039	3.892	0.9263
	CR	21.905	0.033	0.7838	23.611	0.002	0.9106	12.477	0.572	0.6997	3.8351	3.305	0.8941

RhB and CR concentrations increased, indicating that a high initial concentration was favourable for the RhB and CR molecules to diffuse inside the RFB_{550} particles, but $R^2 < 0.71$ and $C \neq 0$, indicating that intra-particle diffusion was not the only rate-limiting step. The Elovich model fit well to the kinetic data, indicating that the adsorption of RhB and CR onto RFB_{550} was not a simple first-order reaction and adsorption was an integrated process controlled by the reaction rate and diffusion (Wu *et al.* 2009), as consistent with the results of the fits to the pseudo-second-order kinetic and intra-particle diffusion models.

Adsorption isotherms and thermodynamics

The sorption equilibrium data obtained at different temperatures were analysed using the Langmuir and Freundlich models. The results are shown in Figure 4 and Table 3. The adsorption reached equilibrium when the initial concentrations of RhB and CR were 30 mg · L^{-1} and 20 mg · L^{-1}, respectively. Coefficient of correlation indicated that the Freundlich model ($R^2 > 0.95$) described the adsorption process well. The adsorption of RhB and CR onto RFB_{550} was therefore a multi-molecular layer adsorption

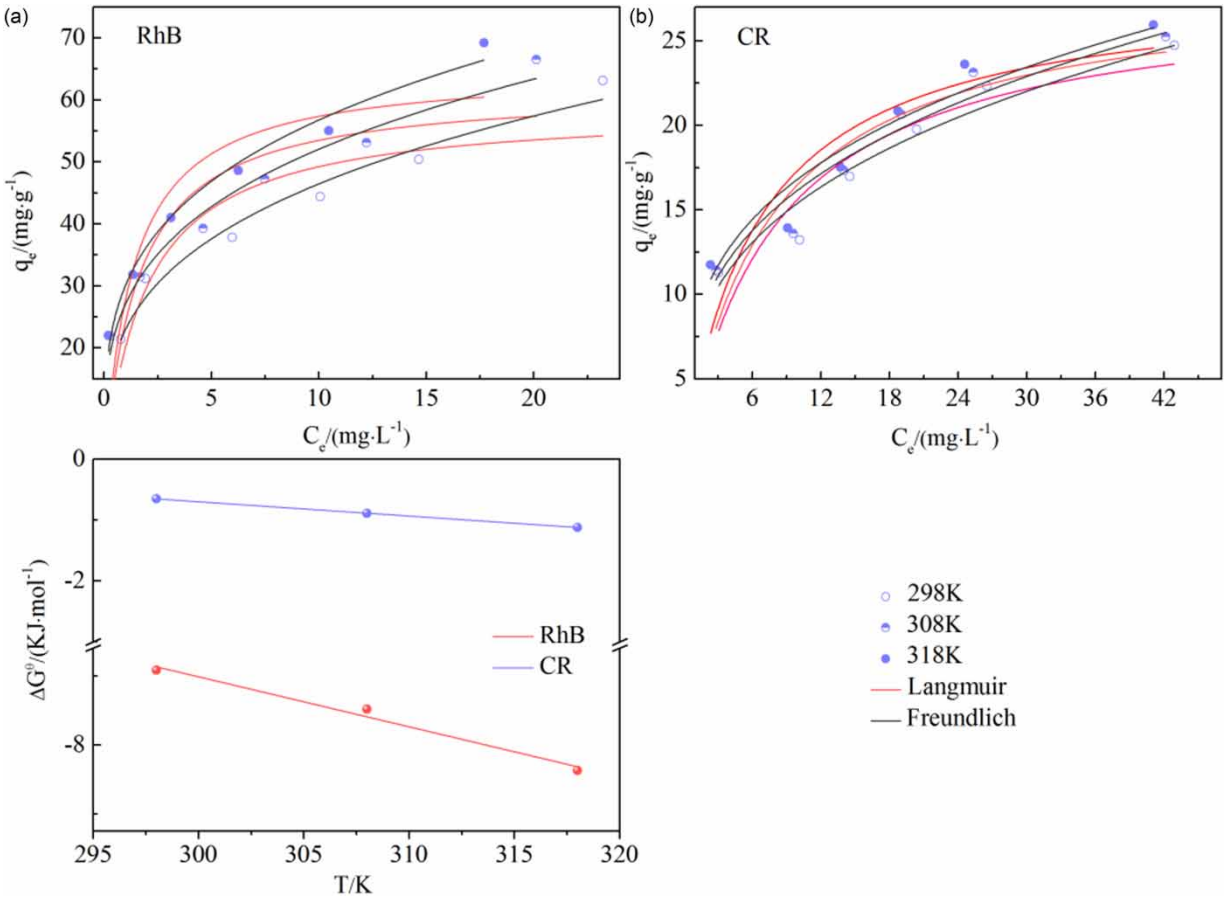

Figure 4 | Isothermal and thermodynamic adsorption curves of RhB and CR onto RFB_{550}.

process, and the amount adsorbed would continue to increase when the concentration of adsorbate was high (Delle Site 2001). This finding was consistent with the results of the fits to the kinetic models. In addition, the constant K_F positively reflected the adsorption capacity. In this study, the K_F value of RhB was higher than CR, indicating that the adsorption capacity of RFB_{550} for RhB was greater than CR. The factor 1/n reflected the surface homogeneity of adsorption. Values of $1/n < 0.5$ indicate that the adsorption process was easily completed, whereas values of $1/n > 2$ indicate that the adsorption process was more difficult to complete (Shi *et al.* 2014). In the present study, the values of 1/n for RhB and CR were all lower than 0.33, indicating that the adsorption of RhB and CR onto RFB_{550} readily occurred.

Thermodynamic fitting results are shown in Figure 4 and Table 4. The negative values for ΔG at different temperatures suggested that the adsorption of RhB and CR onto RFB_{550} occurred in a spontaneous process. In

Table 3 | Langmuir and Freundlich isotherm parameters for RhB and CR adsorption

		Langmuir model			Freundlich model		
	T/K	q_m	K_L	R^2	K_F	1/n	R^2
RhB	298	58.698	0.521	0.7994	22.990	0.305	0.9642
	308	61.829	0.642	0.6966	27.095	0.283	0.9709
	318	65.029	0.748	0.7305	30.080	0.275	0.9803
CR	298	27.969	0.127	0.8024	7.297	0.325	0.9632
	308	28.559	0.137	0.8058	7.806	0.316	0.9607
	318	28.372	0.157	0.7505	8.396	0.302	0.9553

addition, as the temperature increased a greater decrease was observed in the ΔG values, implying that higher temperatures favour RhB and CR adsorption. The values of ΔS^{θ} and ΔH were positive, indicating that adsorption was an endothermic process characterised by an increase in entropy. Generally, when $4 < \Delta H^{\theta} < 10\ \mathrm{kJ \cdot mol^{-1}}$, the acting force was the van der Waals force; when $2 < \Delta H^{\theta} < 29$, the acting force was the dipole force; and when $2 < \Delta H^{\theta} < 40\ \mathrm{kJ \cdot mol^{-1}}$, the acting force was the hydrogen bond force. We speculated that the adsorption of RhB onto RFB_{550} was primarily mediated by dipole forces and hydrogen bonds. RFB_{550} mainly adsorbs CR through van der Waals forces, dipole forces and hydrogen bonds.

FTIR analysis before and after adsorption

The FTIR spectra of RFB_{550} showed changes in the functional groups on the surfaces of the biochar samples (Figure 5(a)). The absorption peaks at 2,939–2,878 $\mathrm{cm^{-1}}$ were assigned to the C–H stretching vibration of methyl groups. The peaks at 3,322, 1,552 and 1,075 $\mathrm{cm^{-1}}$ were assigned to the stretching vibration of the phenolic –OH, C = C and C = O bonds in the aromatic ring, and C–O bonds in ester and ether groups, respectively, and the peak at 834 $\mathrm{cm^{-1}}$ was assigned to the C–H bond in aromatic and heterocyclic groups (Steinbeiss *et al.* 2009; Zheng *et al.* 2013). The abundance of functional groups and aromatic structures on the surface of RFB_{550} provided a good substrate for the adsorption of RhB and CR.

According to Figure 5(b), some positions of the peaks and peak heights were shifted in the samples containing RhB and CR compared with the FTIR spectra of the biochar alone. The band at 3,322 $\mathrm{cm^{-1}}$ in the RFB_{550} spectrum shifted to 3,574 and 3,562 $\mathrm{cm^{-1}}$, suggesting that hydrogen bonds might form through the interactions of $-CH_3$, –COOH, and N-containing heterocyclic ring in the adsorbate and the oxygen-containing functional groups on RFB_{550}. Therefore, we speculated that hydrogen bonds played an important role in the adsorption process. The characteristic C–H, C=O, C=C and C–O peaks shifted, indicating that the C=O, C=C and C–O groups were all involved in the adsorption process. In addition, the C–H absorption peaks at approximately 834 $\mathrm{cm^{-1}}$ exhibited a blueshift to a lower wave number, which may be associated with the formation of π–π bonds through the interactions of –COOH and the aromatic structure of the adsorbate and the C–H and C=C functional groups on RFB_{550}. After adsorption, the peaks of RhB at 3,500 and 750 $\mathrm{cm^{-1}}$ were obviously stronger than the peaks of CR, and this phenomenon might be one of the explanations for the stronger adsorption of RhB onto RFB than CR.

Table 4 | Thermodynamic parameters for the removal of RhB and CR by RFB_{550}

	ΔG^{θ}				
	298 K	308 K	318 K	ΔH^{θ}	ΔS^{θ}
RhB	−6.921	−7.486	−8.371	14.736	0.073
CR	−0.652	−0.891	−1.121	6.342	0.023

CONCLUSIONS

RFB_{550} was produced from rabbit faeces through pyrolysis and displayed high specific surface area, well-developed

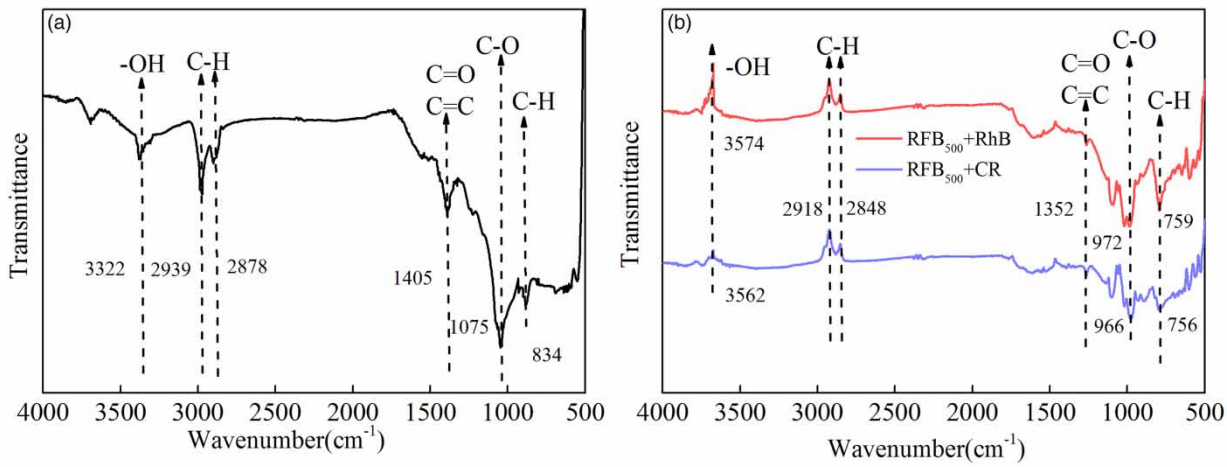

Figure 5 | FTIR spectra recorded before (a) and after (b) RhB and CR adsorption.

porous structure and abundant surface functional groups. The adsorption process of RhB and CR onto RFB_{550} was more accurately described by the pseudo-second-order model and the Freundlich model, and the fitting results showed that the adsorption process was not a single mechanism. The entire process was jointly controlled by liquid film diffusion, surface adsorption and intra-particle diffusion. The calculated thermodynamic parameters indicated that the adsorption of RhB and CR onto RFB_{550} was a spontaneous and endothermic process. According to the FTIR analysis, hydrogen bonds and π–π bonds were intimately involved in the adsorption process. The present study shows the promise of rabbit faeces-derived biochar as an effective adsorbent for the removal of atrazine from aqueous solutions.

REFERENCES

Ahmad, R. & Kumar, R. 2010 Adsorptive removal of Congo red dye from aqueous solution using bael shell carbon. *Applied Surface Science* **257** (5), 1628–1633.

Almasi, A., Omidi, M., Khodadadian, M., Khamutian, R. & Gholivand, M. B. 2012 Lead(II) and cadmium(II) removal from aqueous solution using processed walnut shell: kinetic and equilibrium study. *Toxicological and Environmental Chemistry* **94** (4), 660–671.

Baslak, C., Arslan, G., Kus, M. & Cengeloglu, Y. 2016 Removal of Rhodamine B from water by using CdTeSe quantum dot-cellulose membrane composites. *RSC Advances* **6** (22), 18549–18557.

Bordoloi, N., Dey, M. D., Mukhopadhyay, R. & Kataki, R. 2018 Adsorption of Methylene blue and Rhodamine B by using biochar derived from Pongamia glabra seed cover. *Water Science and Technology* **77** (3), 638–646.

Cheng, Z. L., Li, Y. X. & Liu, Z. 2018 Study on adsorption of rhodamine B onto Beta zeolites by tuning SiO_2/Al_2O_3 ratio. *Ecotoxicology and Environmental Safety* **148**, 585–592.

Dawood, S. & Sen, T. K. 2012 Removal of anionic dye Congo red from aqueous solution by raw pine and acid-treated pine cone powder as adsorbent: equilibrium, thermodynamic, kinetics, mechanism and process design. *Water Research* **46** (6), 1933–1946.

Delle Site, A. 2001 Factors affecting sorption of organic compounds in natural sorbent/water systems and sorption coefficients for selected pollutants. A review. *Journal of Physical and Chemical Reference Data* **30** (1), 187–439.

Fan, S., Tang, J., Wang, Y., Li, H., Zhang, H., Tang, J., Wang, Z. & Li, X. 2016 Biochar prepared from co-pyrolysis of municipal sewage sludge and tea waste for the adsorption of methylene blue from aqueous solutions: kinetics, isotherm, thermodynamic and mechanism. *Journal of Molecular Liquids* **220**, 432–441.

Hameed, B. H. & Ahmad, A. A. 2009 Batch adsorption of methylene blue from aqueous solution by garlic peel, an agricultural waste biomass. *Journal of Hazardous Materials* **164** (2–3), 870–875.

Khattri, S. D. & Singh, M. K. 2009 Removal of malachite green from dye wastewater using neem sawdust by adsorption. *Journal of Hazardous Materials* **167** (1–3), 1089–1094.

Li, L., Liu, S. X. & Zhu, T. 2010 Application of activated carbon derived from scrap tires for adsorption of Rhodamine B. *Journal of Environmental Sciences* **22** (8), 1273–1280.

Lian, F., Cui, G. N., Liu, Z. Q., Duo, L., Zhang, G. L. & Xing, B. S. 2016 One-step synthesis of a novel N-doped microporous biochar derived from crop straws with high dye adsorption capacity. *Journal of Environmental Management* **176**, 61–68.

Mandal, A., Singh, N. & Purakayastha, T. J. 2017 Characterization of pesticide sorption behaviour of slow pyrolysis biochars as low cost adsorbent for atrazine and imidacloprid removal. *Science of the Total Environment* **577**, 376–385.

Schimmelpfennig, S. & Glaser, B. 2012 One step forward toward characterization: some important material properties to distinguish biochars. *Journal of Environmental Quality* **41** (4), 1001–1013.

Sewu, D. D., Boakye, P. & Woo, S. H. 2017 Highly efficient adsorption of cationic dye by biochar produced with Korean cabbage waste. *Bioresource Technology* **224**, 206–213.

Shi, L., Zhang, G., Wei, D., Yan, T., Xue, X. D., Shi, S. S. & Wei, Q. 2014 Preparation and utilization of anaerobic granular sludge-based biochar for the adsorption of methylene blue from aqueous solutions. *Journal of Molecular Liquids* **198**, 334–340.

Steinbeiss, S., Gleixner, G. & Antonietti, M. 2009 Effect of biochar amendment on soil carbon balance and soil microbial activity. *Soil Biology & Biochemistry* **41** (6), 1301–1310.

Sun, Y. B., Ding, C. C., Cheng, W. C. & Wang, X. K. 2014 Simultaneous adsorption and reduction of U(VI) on reduced graphene oxide-supported nanoscale zerovalent iron. *Journal of Hazardous Materials* **280**, 399–408.

Wu, F. C., Tseng, R. L. & Juang, R. S. 2009 Characteristics of Elovich equation used for the analysis of adsorption kinetics in dye-chitosan systems. *Chemical Engineering Journal* **150** (2–3), 366–373.

Yang, G. X. & Jiang, H. 2014 Amino modification of biochar for enhanced adsorption of copper ions from synthetic wastewater. *Water Research* **48**, 396–405.

Zhang, J. H., Yan, Z. L., Ouyang, J., Yang, H. M. & Chen, D. L. 2018 Highly dispersed sepiolite-based organic modified nanofibers for enhanced adsorption of Congo red. *Applied Clay Science* **157**, 76–85.

Zhang, Z. Y., Moghaddam, L., O'Hara, I. M. & Doherty, W. O. S. 2011 Congo Red adsorption by ball-milled sugarcane bagasse. *Chemical Engineering Journal* **178**, 122–128.

Zheng, H., Wang, Z. Y., Deng, X., Zhao, J., Luo, Y., Novak, J., Herbert, S. & Xing, B. S. 2013 Characteristics and nutrient values of biochars produced from giant reed at different temperatures. *Bioresource Technology* **130**, 463–471.

First received 27 July 2019; accepted in revised form 24 February 2020. Available online 4 March 2020